PAPER

Development of a Simple and Lightweight Phantom for Evaluating Human Body Avoidance Technology in Microwave Wireless Power Transfer

Kazuki SATO[†], ***Student Member and*** **Kazuyuki SAITO**[†a)], ***Member***

SUMMARY In recent years, microwave wireless power transfer (WPT) has attracted considerable attention due to the increasing demand for various sensors and Internet of Things (IoT) applications. Microwave WPT requires technology that can detect and avoid human bodies in the transmission path. Using a phantom is essential for developing such technology in terms of standardization and human body protection from electromagnetic radiation. In this study, a simple and lightweight phantom was developed focusing on its radar cross-section (RCS) to evaluate human body avoidance technology for use in microwave WPT systems. The developed phantom's RCS is comparable to that of the human body.

key words: *microwave, wireless power transfer, radar cross-section, human body avoidance, simple and lightweight phantom*

1. Introduction

1.1 Microwave Wireless Power Transfer

With the expansion of the Internet of Things (IoT) in recent years, the number of small sensors, small cameras, and other smart devices have increased exponentially, increasing the need to realize an Internet of Energy society (IoE) [1]. Microwave wireless power transfer (WPT) is a promising next-generation power supply system [2]. It has the advantage of a relatively long transmission range, which makes it possible to eliminate battery replacement and disposal and power supply wiring, thus eliminating the need for conscious charging and supplying power [3], [4]. On the other hand, its low-power transmission and low efficiency are serious disadvantages. To resolve these issues, a power transmission method that avoids human bodies in the transmission path can be used [5]. Human body avoidance technology is also important from the viewpoint of human body protection. However, during its development, using actual human bodies is undesirable because of the uncertainty of the acquired data and the risks associated with exposure to electromagnetic radiation. Therefore, a human body phantom should be used when evaluating WPT transmitters.

The WPT transmitter was assumed to be installed on a ceiling and to detect human bodies based on radio wave backscattering by a human body. The frequency was 920 MHz, which has been used in microwave WPT [6]. As shown in Fig. 1, the phantom was placed on a mobile robot and moved freely within the irradiation range of the WPT transmitter to evaluate the performance of human body avoidance. Considering the microwave WPT beam size for evaluating the actual WPT transmitter, the phantom should be about the same size as the human body. Although various human body phantoms have been developed, they are made by filling human body–shaped molds with insulating rubber or gel-like materials, which are not suitable for evaluation because they are so heavy to move easily [7], [8]. Therefore, in this study, a simple and lightweight phantom that scatters radio waves as much as the human body was developed.

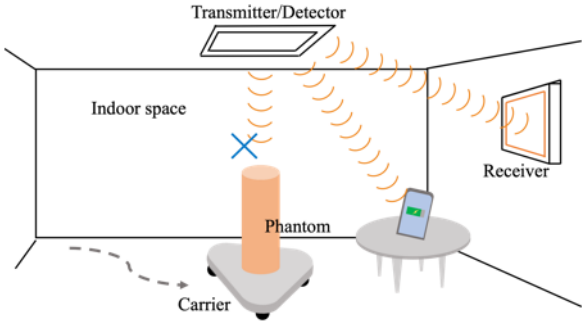

Fig. 1 Phantom Usage Assumptions.

1.2 Radar Cross Section

The phantom was developed by focusing on the radar cross-section (RCS), which is an indicator of the degree of radio wave scattering by an object. It is used in anti-collision radar for automobiles, ship and aircraft radar, weather observation, and other applications, and is an important element for object detection. The RCS is calculated as

$$\mathrm{RCS} = 4\pi R^2 \left| \frac{E_{scat}}{E_{in}} \right| \tag{1}$$

where E_{in} is the electric field strength of the incident wave (V/m), E_{scat} is the electric field strength of the scattered wave (V/m), and R is the distance between the antenna and the object (m) [9]. In general, when the directions of the incident and scattered waves coincide, it is called monostatic RCS (hereinafter, simply called RCS), which is an important

Manuscript received September 14, 2022.
Manuscript revised December 22, 2022.
Manuscript publicized February 15, 2023.
[†]The authors are with Chiba University, Chiba-shi, 263-8522 Japan.
a) E-mail: kazuyuki_saito@faculty.chiba-u.jp
DOI: 10.1587/transcom.2022EBP3155

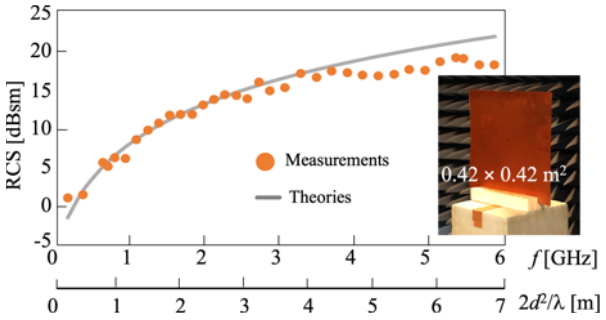

Fig. 2 Measurement results of conductor plate.

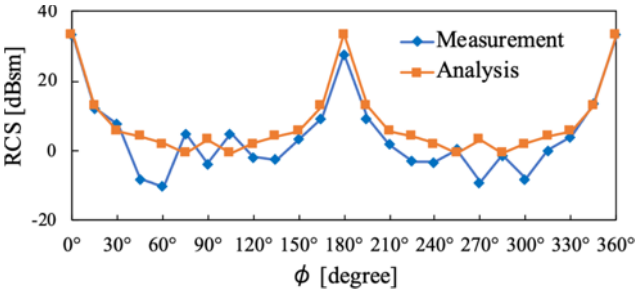

Fig. 3 RCS measurement results for scaled conductor plate model.

indicator for evaluating radar performance.

The RCS of an object can generally be expressed by Eq. (2) from the radar range equation [10].

$$\mathrm{RCS} = \frac{P_r}{P_t}\frac{(4\pi)^3 R^4}{G_t G_r \lambda^2} \tag{2}$$

where λ is the wavelength of the incident wave (m), P_r is the received power by receiving antenna (W), P_t is the transmitted power by transmitting antenna (W), R is the distance between the antenna and the target (m), G_t is the gain of the transmitting antenna, and G_r is the gain of the receiving antenna.

The RCS has been actively studied and various measurement methods have been developed [11]. The RCS can be measured simply by using a vector network analyzer (VNA) when the wavelength of the incident wave, the distance between the antenna and the target, the gain of the transmitting antenna, and the gain of the receiving antenna are known, since it is expressed as the ratio of the transmitting and receiving power in Eq. (2). In this case, to observe only the wave reflected from the measurement target, it is necessary to remove unwanted waves reflected from the anechoic chamber or the antenna. For separation, gating processing with the time domain function can be used [12].

Figure 2 shows the RCS measurement results using this measurement method and the theoretical values for a conductor plate, along with the ratio of the wavelength to the length of one side of the conductor plate. The measurement results were normalized to 1 m^2. The theoretical RCS value of a conductive flat plate is expressed by Eq. (3) based on its shape [10].

$$\mathrm{RCS} = \frac{4\pi w^2 h^2}{\lambda^2} \tag{3}$$

where λ is the wavelength of the incident wave (m), and w and h are the width and height of the conductor plate, respectively (m). The measurement conditions were as follows: conductor plate, 0.42×0.42 m^2; antenna, LPDA-USLP9142 (Schwarzbeck Mess-Elektronik, Schönau, Germany), VNA, N5230C (Agilent Technologies, Santa Clara, CA, USA).

The measurement results were in good agreement with the theoretical values in the range of 800 MHz–6 GHz, confirming the validity of the measurement method. However, it should be noted that the differences between the measured and theoretical values will be greater if the measurement environment does not strictly satisfy the far-field condition. Even in the measurement environment used, the differences became greater when the distance between the antenna and the target ($R = 3.6$ m) was less than $2d^2/\lambda$. The d is the size of the aperture plane of the flat plate (420 mm × 420 mm^2), λ is the wavelength at the measured frequency (320 mm), and $d = wh$ in Eq. (3). This means that the larger the object to be measured, the longer the measurement distance should be.

When the measurement objects are large, such as ship and aircraft, RCS measurements are performed using a scaled model. It is irradiated radio waves of a wavelength corresponding to their scale ratio. Using a scale model, the RCS of a 2×2 m^2 conductor plate at 1 GHz was measured. In Fig. 3, the analytical results were obtained using XFdtd (Remcom, State College, PA, USA), electromagnetic field analysis software based on the finite-difference time-domain method. A 0.35×0.35 m^2 conductor plate was used for the scaled model (scale ratio: 0.175), and the irradiation frequency was 5.7 GHz. To meet the far-field requirement, a distance of about 27 m between the antenna and the conductor plate was initially needed. The use of the scaled model reduced the required distance to 4.7 m. Although the distance in this measurement environment was only 3.6 m, the measurement and analytical values were in sufficiently good agreement, indicating that the scaled model was suitable. Given the above, a phantom was developed considering the RCS of the human body and was evaluated through measurements and analyses using the scaled model.

2. RCS Analysis of Human Body Models

Previous studies have reported that the RCS of the human body depends on the frequency, irradiation angle, and polarization of the radio wave [13]–[15]. However, there has been insufficient research on RCS assuming irradiation from above the human body, as in the case of microwave WPT. Therefore, in this study, the RCS was investigated assuming radio wave irradiation from above the human body, and the phantom's RCS values were calculated accordingly.

2.1 RCS Variation in the Human Body

Assuming radio wave irradiation from above, the human

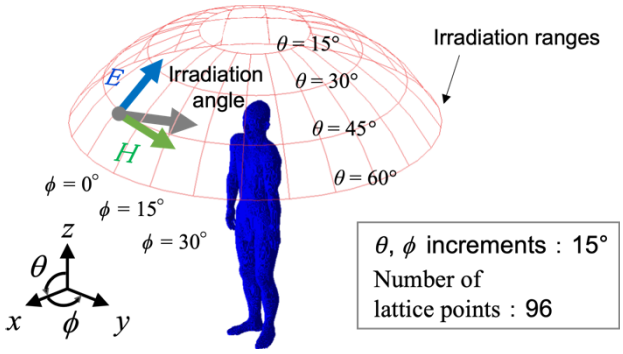

Fig. 4 Analysis Model.

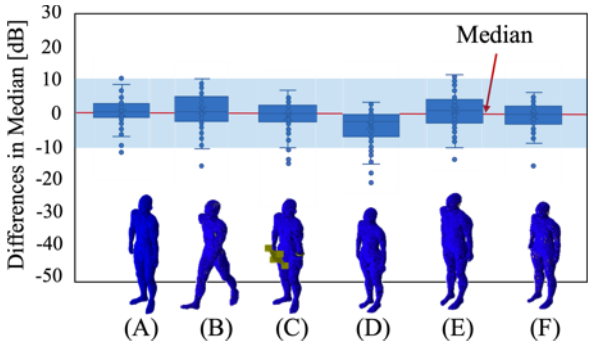

Fig. 5 Box-and-whisker diagram. Each model is plotted on the horizontal axis, and the vertical axis plots the difference between the median RCS and each model's RCS at all calculated grid points.

body's RCS is mostly in the range of −15 to −9 dBsm [16]. However, it may vary depending on personal belongings, body shape, and other factors. Therefore, its variation was calculated using various human body models. Here, investigating RCS using an actual human body is not appropriate due to inaccuracies in measurements and ethical considerations, so that the RCS of a human body is calculated numerically.

The WPT transmitter installed on the ceiling feeds the entire room with a transmission range at a 30–90° depression angle [17]. This means that the human body is irradiated from a zenith angle of 0–60°. Therefore, an umbrella-shaped range of $15° \leq \theta \leq 60°$ and $0° \leq \phi \leq 360°$ was used as the radio wave coverage area (Fig. 4). The radio waves were emitted from the normal direction of 96 grid points obtained by changing the angle of incidence in increments of 15°, and the RCS was calculated for each irradiation direction. E-polarized plane waves at 920 MHz were used as the incident waves. XFdtd was used for the calculations. The cell size was $2 \times 2 \times 2$ mm^3, and the absorbing boundary consists of seven perfectly matched layers.

Six different human body models were used: a walking man (model B in Fig. 5), a man wearing a wristwatch and holding a tablet (model C), a standing man (model A, model E), and a standing woman (model D, model F). Model A and D are high-definition numerical human body models — Taro (male) and Hanako (female) — developed by National Institute of Information and Communications Technology [18]. Model E and F are high-definition numerical human body models — Duke (male) and Ella (female) — developed by the IT'IS Foundation [19].

It should be noted that the Earth may exert an influence on the WPT transmitter, depending on the use setting. However, its influence is not expected to change the RCS of the phantom or the human body itself. Therefore, to save computational resources, this influence was not considered.

Figure 5 is a box-and-whisker diagram showing the difference between each human body model's RCS and the median RCS of the six models. The obtained RCSs were normalized to 1 m^2, and the difference was expressed in dB. About 90% of each model's RCS was within ±10 dB of the median RCS value. A comparison of the variations between model A and B and between model A and C showed that the variation between model A and B was greater than that between model A and C. This suggests that differences in posture, such as when walking, affect the variation in RCS more than differences in electrical characteristics, such as personal belongings. Due to their smaller sizes, females (model D, F) had smaller RCSs than males (model A, E).

The above results suggest that the variation in the human body's RCS is about ±10 dB. For consistency with this range, the phantom was developed based on the median RCS value of the six human body models.

2.2 RCS Calculation of Human Body Models of Different Shapes

A phantom that scatters radio waves to the same degree as the human body can be produced by filling a container in the shape of a human body with gel. However, this is not realistic because its weight is equivalent to that of a human body, and its fabrication is not easy. Thus, in this study, a phantom of an appropriate size and weight was fabricated.

As mentioned in Sect. 1, the size of the phantom should be about the same as that of the human body, considering the beam size of actual microwave WPT device. Therefore, its height should be set at about 1.73 m about the same as that of the human body model Taro [18].

Figure 6 shows the RCS calculation results for human body models A and B. Model A is the Taro model without the head, and model B is the same model without the arms. A color map shows the differences between the RCS of the full-body Taro model and those of models A and B. As shown in Fig. 6(a), the differences were greater around ϕ = 90–270° at θ = 15°, indicating that the RCS around the neck is difficult to reproduce if the head shape is eliminated. As shown in Fig. 7(b), the differences were greater around ϕ = 30–60° and 315–345°, indicating that with a narrow shoulder width, it is difficult to reproduce the RCS in a diagonal forward direction. The average RCS difference was −3.37 dB, suggesting a small overall RCS. These results indicate that the width of the head and shoulders contributes significantly to the human body's RCS.

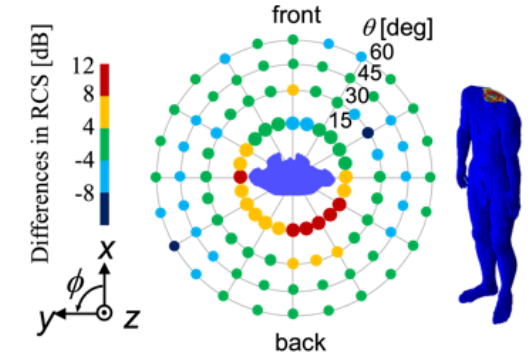

(a) Model A (Taro without head)

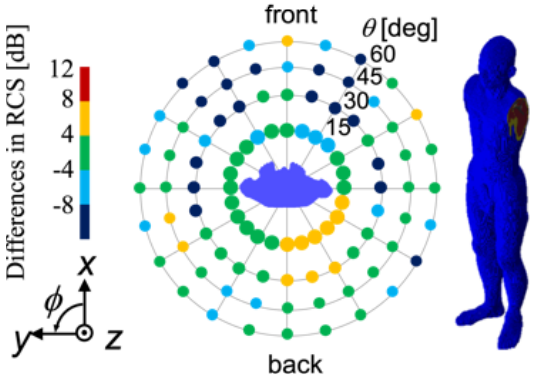

(b) Model B (Taro without arms)

Fig. 6 RCS calculation results of human body model A and B.

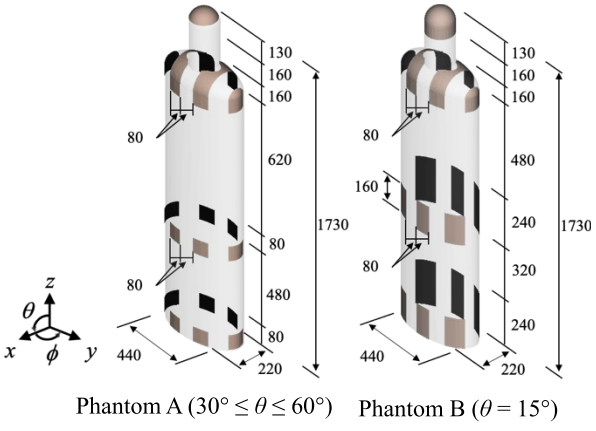

Fig. 7 Phantom models.

3. Phantom Development

Under the geometrical conditions identified in Sect. 2, the two phantoms shown in Fig. 7 were fabricated. These phantoms consisted of a head composed of a cylinder with a 70 mm radius and a hemisphere with a 70 mm radius, a body composed of an elliptic cylinder 440 mm major axis, 220 mm minor axis, and 1350 mm high, and a shoulder composed of an elliptic sphere 100 mm high and with the same diameter as the body, to which scatterers were attached. The

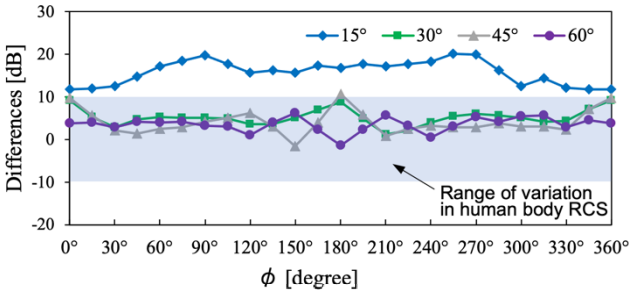

(a) Phantom A

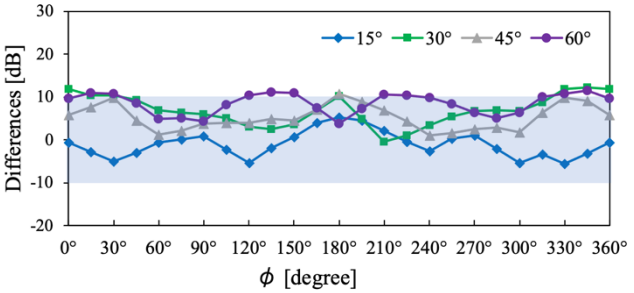

(b) Phantom B

Fig. 8 RCS calculation result. The graph (a) shows the results for Phantom A and the graph (b) shows the results for Phantom B. On the vertical axis, the difference in RCS from the median RCS value of the six human models (described in Sect. 2.2) is displayed for each irradiation angle θ. The blue bands represent the range of variation in the RCS of the human body.

base was made of a very lightweight material, polystyrene foam, and the RCS was controlled by the pattern of the scatterers attached to the base. The above various dimensions were set based on the values of the human body model Taro.

The phantoms' RCSs were calculated under the conditions described in Sect. 2. The base was defined as free space, and the scatterers were thin-film perfect electric conductors. The results are shown in Fig. 8. The phantoms' RCS values were generally close to the target values. Specifically, the RCS was within ±10 dB of the target values in the θ = 30–60° direction for phantom A and the θ = 15 and 45° directions for phantom B. Thus, the phantoms had RCSs equivalent to that of the human body when irradiated from these directions. Therefore, by using Phantom A when θ = 30–60° and Phantom B when θ = 15°, the irradiation range of the WPT transmitter can be covered and can be used to evaluate human body avoidance technologies.

The fabricated phantoms are shown in Fig. 9. The phantoms were lightweight (2.97 kg) due to the use of polystyrene foam as the base and copper foil tape as the scatterer. RCS measurements were performed for phantoms A and B. Because the phantoms were too large to obtain sufficient irradiation angles and distances in the anechoic chamber, the measurements were performed using models scaled to 1/3. A schematic of the measurement environment is shown in Fig. 10. The measurement equipment used was described in Sect. 1. The VNA settings were as follows: IF bandwidth, 50 kHz; frequency range, 0.76–7.76 GHz; number of points, 1601.

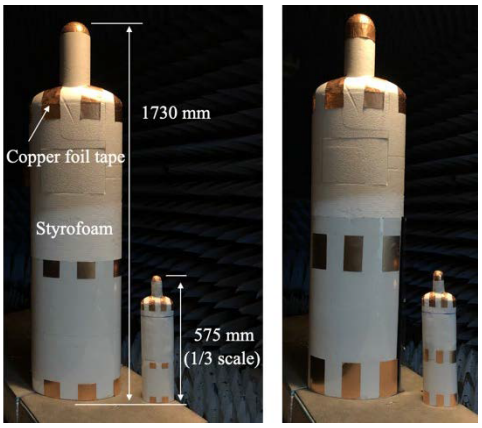

Fig. 9 Fabricated Phantom with scale model.

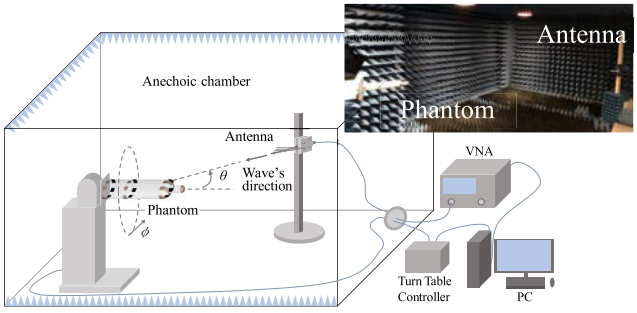

Fig. 10 RCS measurement environment.

The difference between the RCS measurement results of the phantoms and the RCS calculated results of the human model is shown in Fig. 11. The results show that the RCS of Phantom A is within the range of variation of the RCS of the human body in the range of $\theta = 30$ to $60°$ as in the analytical results in Fig. 8. On the other hand, Phantom B is not within the range of variation of the RCS of the human body in the range of $\theta = 15°$ direction.

In Fig. 12, the measurement results at $\theta = 15°$ and $60°$ for phantoms A and B are shown for comparison with the analytical results. The same trend as in the analysis was observed for almost all irradiation angles. At some points, the difference was as large as 5 dB because the wave reflected from the phantom was close to the floor noise level. The floor noise was about −90 dB in each situation, and the reflection coefficient at the phantom was expected to be about −70 to −85 dB. Therefore, floor noise caused a certain variation. For the same reason, in the $\theta = 15°$ direction for phantom B, the wave reflected from the phantom was smaller than the floor noise, so the distribution differed from that in the analysis. However, despite these variations, the RCS trend of the scaled models was generally similar to that obtained from the analysis. A similar trend was also observed for $\theta = 30°$ and $45°$ (not shown here). This suggests that the fabricated phantoms exhibited the same RCS trend as in the analysis in a real environment. This suggests that the RCS

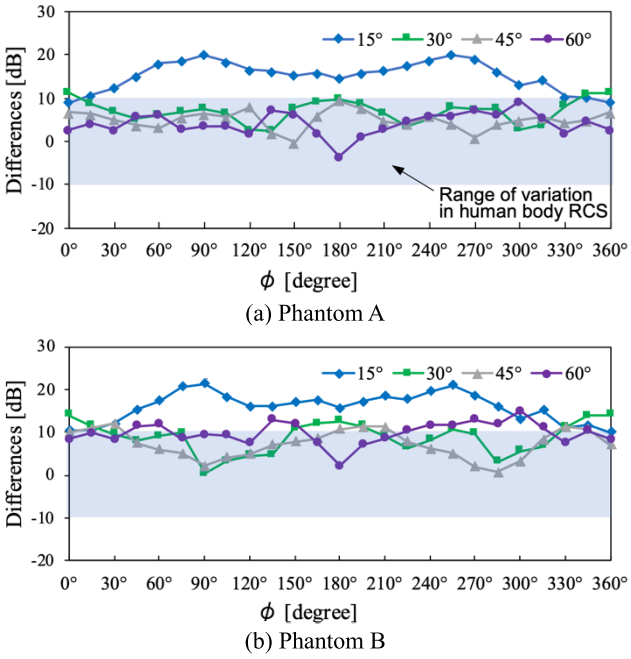

Fig. 11 RCS measurement results. The graph (a) shows the results for Phantom A and the graph (b) shows the results for Phantom B. On the vertical axis, the difference in RCS from the median RCS value of the six human models (described in Sect. 2.2) is displayed for each irradiation angle θ. The blue bands represent the range of variation in the RCS of the human body.

of $\theta = 15°$ for fabricated phantom B is comparable as the RCS of human body the same as analysis although the RCS could not be measured correctly because it is smaller than the limit of the measurement setup. Thus, it can be said that fabricated Phantoms A and B have an RCS comparable to that of the human body.

4. Conclusion

In this work, a simple and lightweight phantom was developed for evaluating human body avoidance technology for microwave WPT. Calculations showed that the RCS varies between human bodies by approximately ±10 dB. To reproduce the RCS of a human body, a head shape and two shoulder parts are necessary, and even if they are simplified to the greatest possible extent, a kokeshi-like shape is necessary. A lightweight phantom was fabricated by attaching copper foil tape to the base of the kokeshi-like styrofoam. This represents a novel phantom fabrication method.

The analysis and measurement results showed that the phantoms' RCSs were within the human body's RCS range. In other words, the fabricated phantoms scatter radio waves to the same degree as the human body. In the future, we plan to verify the effectiveness of these phantoms by conducting human avoidance experiments using a microwave WPT system.

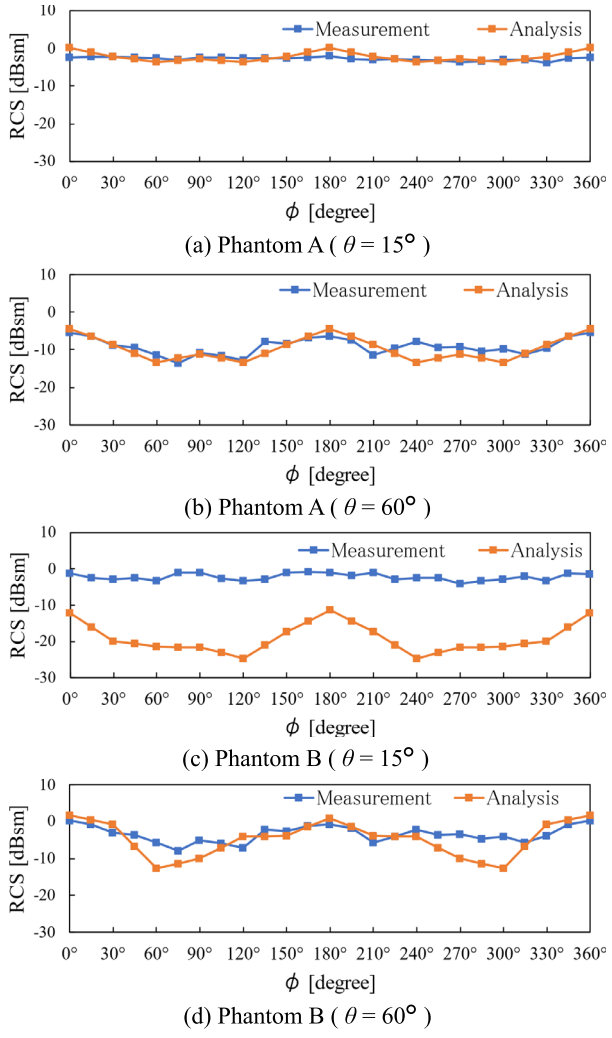

(a) Phantom A ($\theta = 15°$)

(b) Phantom A ($\theta = 60°$)

(c) Phantom B ($\theta = 15°$)

(d) Phantom B ($\theta = 60°$)

Fig. 12 RCS measurement result.

Acknowledgments

This work is supported by Cabinet Office, Government of Japan, Cross-ministerial Strategic Innovation Creation Program (SIP) "WPT Systems for Sensor Networks and Mobile Equipment (Indoor Power Supply)" (Management Corporation: Japan Science and Technology Agency, JST).

References

[1] Y.R. Kafle, K. Mahmud, S. Morsalin, and G.E. Town, "Towards an internet of energy," 2016 IEEE Int. Conf. Power Syst. Tech., Delhi, India, pp.1–6, March 2016.

[2] H. Shahinzadeh, J. Moradi, G.B. Gharehpetian, H. Nafisi, and M. Abedi, "Internet of energy (IoE) in smart power systems," 2019 5th Conference on Knowledge Based Engineering and Innovation (KBEI), Tehran, Iran, pp.627–636, Feb. 2019.

[3] S. Kim, C. Mariotti, F. Alimenti, P. Mezzanotte, A. Georgiadis, A. Collado, L. Roselli, and M.M. Tentzeris, "No battery required: Perpetual RFID-enabled wireless sensors for cognitive intelligence applications," IEEE Microw. Mag., vol.14, no.5, pp.66–77, July-Aug. 2013.

[4] S. Yoshida, N. Hasegawa, and S. Kawasaki, "Experimental demonstration of microwave power transmission and wireless communication within a prototype reusable spacecraft," IEEE Microw. Wireless Compon. Lett., vol.25, no.8, pp.556–558, Aug. 2015.

[5] L. Ginting, H.S. Yoon, D.I. Kim, and K.W. Choi, "Beam avoidance for human safety in radiative wireless power transfer," IEEE Access, vol.8, pp.217510–217525, 2020.

[6] "Technical condition of in-room far-field wireless power transfer," [online] Available: https://www.soumu.go.jp/main_content/000697268.pdf, July 2020 (in Japanese).

[7] T. Onishi, R. Ishida, T. Takimoto, K. Saito, S. Uebayashi, M. Takahashi, and K. Ito, "Biological tissue-equivalent agar-based solid phantoms and SAR estimation using the thermographic method in the range of 3–6 GHz" IEICE Trans. Commun., vol.E88-B, no.9, pp.3733–3741, Sept. 2005.

[8] T. Hikage, Y. Sakaguchi, T. Nojima, and Y. Koyamashita, "Development of lightweight solid phantom composed of silicone rubber and carbon nanotubes," 2007 IEEE Int. Symp. on Electromagn. Compat., Honolulu, USA, no.9830160, July 2007.

[9] M.I. Skolnik, RADAR HANDBOOK, 2nd ed., pp.320–321, McGraw-Hill Professional, 1990.

[10] C.A. Balanis, Antenna Theory: Analysis and Design, 2nd ed., pp.88–90, John Wiley & Sons, 1997.

[11] D.W. Hess, "Introduction to RCS measurements," 2008 Loughborough Antennas Propag. Conf., Loughborough, UK, pp.37–44, March 2008.

[12] K. Schubert and J. Werner, "One-antenna method with time domain gating using equi-ripple FIR filter," 2020 Int. Symp. Electromagn. Compat. - EMC EUROPE, Rome, Italy, pp.1–3, Sept. 2020.

[13] C. Fang, Y. Qin, and C. Hu, "Numerical study of human head RCS and SAR at 0.9–2.45 GHz," 2017 Int. Appl. Comput. Electromagn. Soc. Symp., Suzhou, China, pp.1–2, Aug. 2017.

[14] E. Piuzzi, P.D. Atanasio, S. Pisa, E. Pittella, and A. Zambotti, "Complex radar cross section measurements of the human body for breath-activity monitoring applications," IEEE Trans. Instrum. Meas., vol.64, no.8, pp.2247–2258, Aug. 2015.

[15] M. Cavagnaro, E. Pittella, and S. Pisa, "Numerical evaluation of the radar cross section of human breathing models," Appl. Comput. Electromagn. Soc. J., vol.30, no.12, pp.1354–1359, Dec. 2015.

[16] M. Suzuki and K. Saito, "Evaluations method of human RCS for simplified phantom development aiming at human body detection," IEICE Trans. Commun. (Japanese Edition), vol.J104-B, no.7, pp.650–652, July 2021.

[17] "Technical condition of in-room far-field wireless power transfer," [online] Available: https://www.soumu.go.jp/main_content/000691546.pdf, July 2020.

[18] T. Nagaoka, S. Watanabe, K. Sakurai, E. Kunieda, S. Watanabe, M. Taki, and Y. Yamanaka, "Development of realistic highresolution wholebody voxel models of japanese adult male and female of average height and weight, and application of models to radio-frequency electromagnetic-field dosimetry," Phys. Med. Biol., vol.49, no.1, pp.1–15, Jan. 2004.

[19] A. Christ, W. Kainz, E.G. Hahn, K. Honegger, M. Zefferer, E. Neufelf, W. Rascher, R. Janka, W. Beautz, J. Chen, B. Kiefer, P. Schmitt, H.P. Hollenbach, J. Shen, M. Oberle, D. Szczerba, A. Kam, J.W. Guag, and N. Kuster, "The virtual family — development of surface-based anatomical models of two adults and two children for dosimetric simulations," Phys. Med. Biol., vol.55, no.2, pp.23–38, Dec. 2009.

Kazuki Sato was born in Fukushima, Japan, in 1996. He received the B.E. degrees in Medical Engineering from Chiba University, Chiba, Japan, in 2021. He is currently the M.E. course at Chiba University, engaging in the research on development of a simple and lightweight phantom for evaluation of human avoidance technology in microwave WPT.

Kazuyuki Saito was born in Nagano, Japan, in 1973. He received the B.E., M.E., and D.E. degrees in Electronic Engineering from Chiba University, Chiba, Japan, in 1996, 1998 and 2001, respectively. He is currently an Associate Professor with the Center for Frontier Medical Engineering, Chiba University. His main interest is in the area of medical applications of electromagnetic field including thermal treatment of cancer and microwave surgical devices etc. Dr. Saito is a member of the Institute of Electrical and Electronics Engineers (IEEE), Institute of the Image Information and Television Engineers of Japan (ITE), the Japanese Society for Thermal Medicine (JSTM), and the Japan Society for Endoscopic Surgery (JSES). He received the IEICE AP-S Freshman Award, the Award for Young Scientist of URSI General Assembly, the IEEE AP-S Japan Chapter Young Engineer Award, the Young Researchers Award of IEICE, and the International Symposium on Antennas and Propagation (ISAP) Paper Award in 1997, 1999, 2000, 2004, and 2005 respectively.